Article

# Fast, High-Throughput Creation of Size-tunable Micro, Nanoparticle Clusters via Evaporative Self-Assembly in Picoliter-Scale Droplets of Particle Suspension

Sun Choi, Arash Jamshidi, Tae Joon Seok, Ming C. Wu, Tarek I Zohdi, and Albert P. Pisano

*Langmuir*, **Just Accepted Manuscript** • DOI: 10.1021/la204362s • Publication Date (Web): 19 Jan 2012

# Fast, High-Throughput Creation of Size-tunable Micro, Nanoparticle Clusters via Evaporative Self-Assembly in Picoliter-Scale Droplets of Particle Suspension

*Sun Choi*[*,1,2], *Arash Jamshidi*[1,3], *Tae Joon Seok*[1,3], *Ming C. Wu*[1,3], *Tarek I. Zohdi*[2] *and Albert P. Pisano*[1,2,3]

[1]Berkeley Sensor and Actuator Center (BSAC), University of California at Berkeley, Berkeley, California 94720, USA

[2]Department of Mechanical Engineering, University of California at Berkeley, Berkeley, California 94720, USA

[3]Department of Electrical Engineering and Computer Science, University of California at Berkeley, Berkeley, California 94720, USA

To whom correspondence should be addressed. E-mail: sunchoi@eecs.berkeley.edu

Berkeley Sensor and Actuator Center (BSAC), University of California at Berkeley, Berkeley, California 94720, USA, Tel: 510-643-9752, Fax: 510-643-6637, E-mail: sunchoi@eecs.berkeley.edu

**RECEIVED DATE (to be automatically inserted after your manuscript is accepted if required according to the journal that you are submitting your paper to)**

ABSTRACT

We report a fast, high-throughput method to create size-tunable micro, nanoparticle clusters via evaporative assembly in picoliter-scale droplets of particle suspension. Mediated by gravity force and surface tension force of a contacting surface, picoliter-scale droplets of the suspension are generated from a nano-fabricated printing head. Rapid evaporative self-assembly of the particles on a hydrophobic surface leads to fast clustering of micro, nanoparticles and forms particle clusters of tunable sizes and controlled spacing. The evaporating behavior of the droplet is observed in real-time and the clustering characteristics of the particles are understood based on the physics of evaporative-assembly. With this method, multiplex printing of various particle clusters with accurate positioning and alignment are demonstrated. Also, size-unifomity of the cluster arrays is thoroughly analyzed by examining the metallic nanoparticle cluster-arrays based on Surface Enhanced Raman Spectroscopy (SERS).

KEYWORDS: Evaporative self-assembly, Microparticle, Nanoparticle Cluster, Picoliter droplets, Fast assembly, Low particle volume fraction, Gravity, Surface tension, SERS

BRIEFS (WORD Style “BH_Briefs”). If you are submitting your paper to a journal that requires a brief, provide a one-sentence synopsis for inclusion in the Table of Contents.

In cutting-edge material science, significant efforts are made to manipulate, locate, and assemble micro, nanoparticles in targeted areas for numerous applications such as three-dimensional photonic crystals[1-3], circuitry of printed electronics on flexible substrates[4, 5], conductometric[6-8], and plasmonic-based biochemical sensors[9, 10]. Conventional approaches to create micro, nanoparticle assemblies - inkjet printing[11-13], electrohydrodynamic jet printing[14], dip-pen lithography[15], Light-actuated dynamic

patterning[16], gravure printing[17], template assisted evaporative self-assembly[18-20] or atomic force microscopy (AFM) tip-based contact printing[21-23] – have achieved a number of milestones in certain applications, however, these methods still suffer from many obstacles such as: long process time (> several minutes)[4, 11, 14-17, 22-29], low throughput,[11, 14-16] complicated and costly set-up,[11, 14, 15] difficult control of pattern size and resolution[11, 14, 15, 17-21, 26] and challenges in an accurate alignment with other features.[11, 14-19, 21-23] Also, large volume consumption of highly concentrated micro, nanoparticle inks increases material processing cost because the cost is mainly determined by the amount of the original materials used for synthesis and patterning of the inks. Here, we report a fast, high-throughput way to create size-controllable micro, nanoparticle clusters via evaporative self-assembly in picoliter-scale droplets of particle suspension. Mediated by gravity force and surface tension force of a contacting surface, the picoliter-scale droplets were generated on a hydrophobic surface from bulk particle suspension in a nano-fabricated printing head. Rapid evaporative self-assembly of the particles on the surface led to fast clustering of microparticles and nanoparticles and formed particle clusters. Clustering of the particles in picoliter-scale droplets was observed in real-time and studied based on the physics of evaporative-assembly. Arrays of various nanoparticle (zinc oxide, gold nanoparticles) clusters and microparticle (silica, polystyrene microspheres) clusters of controlled sizes and spacing were generated on a flat, hydrophobic substrate via fast evaporative self-assembly. The size of the clusters was tunable from single microparticle-scale (~ 1 μm) to several hundred micro meters. Material consumption for creating clusters was lower than other existing approaches because the volume of the dispensed droplets were picoliter-scale and whole fraction of the particles were completely clustered upon the completion of the evaporation of the droplets. With this method, multiplex printing of various particle clusters with accurate positioning and alignment was demonstrated. Size-uniformity of the created clusters was thoroughly analyzed by examining uniform, large arrays of gold nanoparticle clusters based on Surface Enhanced Raman Spectroscopy (SERS). The SERS measurements showed that size-tunable, large arrays of clusters were created from one-step printing of the presented method.

RESULTS AND DISCUSSION

**Generation of Picoliter-scale Droplets of Particle Suspension**

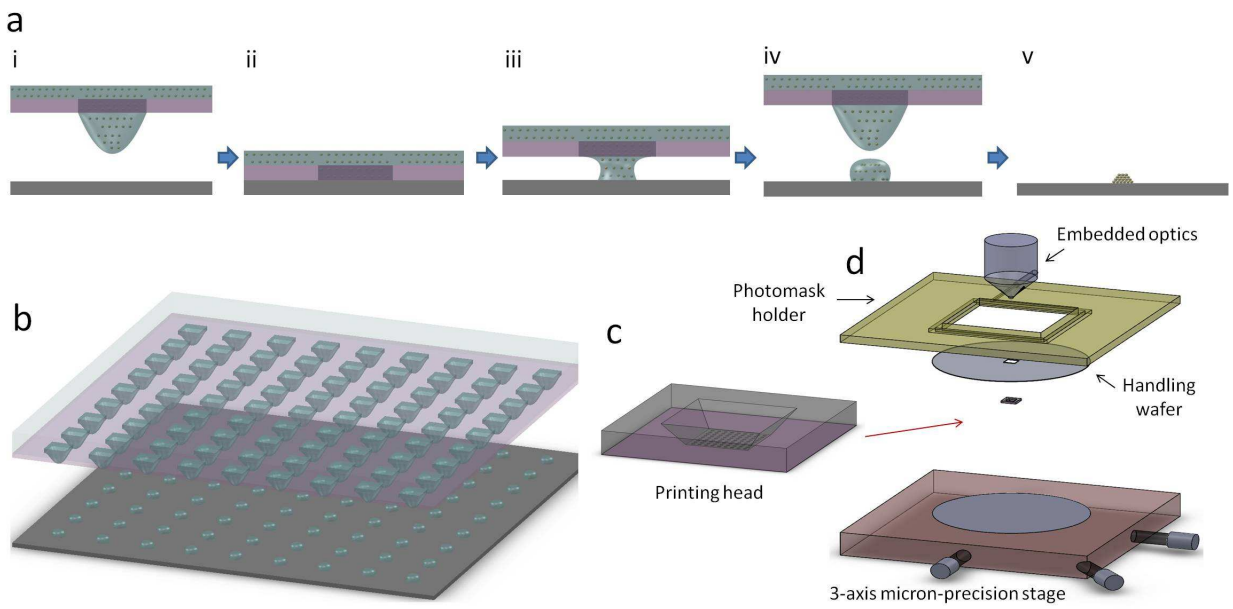


**Figure 1**. Schematics of printing procedure. **a.** Serial processes. (i) Particle suspension menisci are extruded to the upfront end of the membrane by gravity. (ii) Contact of the head with the substrate is achieved. (iii) Surface tension of the substrate attracts a fraction of the suspension fluid. (iv) Picoliter-scale droplets are transferred to the substrate via pinch-off processes. (v) Rapid evaporative self-assembly of the particles forms 3-D clusters. **b,c.** A high-throughput printing head. **d.** A global printing system. A printing head is attached to conventional photolithography tool. 3-axis micron-precision stage and embedded optics performs accurate positioning and alignment of clusters.

Figure 1 illustrates the general procedure of printing micro, nanoparticle clusters. The printing head was fabricated by applying conventional micro-fabrication technology to SOI (Silicon-On-Insulator) substrates. Holes of the printing head were defined by photolithography and reactive-ion-etching was followed. Backside was wet-etched in order to define a reservoir region to contain micro, nanoparticle

suspension. After the final etching step, a microporous membrane with two hundred nanometer thickness was released on the head. It was mechanically robust and did not break by fluid rinsing steps. After the fabrication of a die-size, printing head, the head was attached to a handling wafer and this handling wafer-printing head complex was directly attached to the mask holder of conventional UV-exposure system for photolithography. Micron-precision, three-axis stage controller of the system allocated the printing head to the targeted area aided by the optics in the system. The suspension was loaded by micropipette to the head within a few seconds and the printing head with loaded suspension was covered with a transparent glass cover slip in order to prevent premature drying during the printing processes. Since the patterning of the droplet is not greatly sensitive to the loaded volume of the suspension to the head, the inherent error caused by micropipetting was not considered to be significant. After loading the suspension to the head (0.1 μL ~ 10 μL), meniscus of the droplet was fully extruded to the front end of the head within a second. Direct contact of the head with the substrate was performed to transfer multiple picoliter (2 pL ~ 20 pL)-scale droplets of particle suspension from the bulk suspension to the substrate through porous membranes of the head. This whole printing process takes less than 5 seconds. As illustrated in Figure 1, the printing process of the picoliter-scale droplets is divided into two main steps; a) Extrusion of the meniscus of the fluid and b) Transfer of the droplets to the substrate. The extrusion of fluid meniscus is driven by gravity force. If gravity force drives the fluid by overcoming pressure drop across the membrane, the meniscus is extruded. When the membrane thickness was 10 μm, pressure drop across the membrane with 20 μm × 20 μm cross sectional area was calculated to be on the order of $10^{-1}$ Pa and the meniscus was not extruded. However, when the thickness of the membrane was 200 nm, the pressure drop across the membrane was calculated to be on the order of $10^{-3}$ Pa and gravity drove the fluid meniscus upfront the membrane. The level of extrusion is determined by the competition between inertia force of a droplet and surface tension force of the suspension fluid. In other words, if the gravity force of the fluid outdoes surface tension force of the

fluid, the transfer of the droplets is more inclined to occur. The dimensionless number, Weber number, $We = \frac{\rho V^2 D}{\sigma} = \frac{(\text{Inertia force driven by gravity})}{(\text{Surface tension force})}$ where $\rho$ is the density of the solvent, V is the characteristic velocity of the fluid inside the pore, D is the diameter of the pore and $\sigma$ is the surface tension of the solvent, is a good parameter to analyze the relative force scale of the viscous force to the surface tension force of the fluid. When the width of each pore was 20 μm, the pinch-off and transfer of the droplets from the bulk solvent occurred and the corresponding $We$ was calculated to be on the order of $10^{-8}$. However, when the width of each pore was 4 μm, the droplets were not transferred to the substrate and the corresponding $We$ was calculated to be on the order of $10^{-3}$. It implies that there exists a minimum pore size where the transfer of the droplets from the printing head can be achieved. After the extrusion of the droplet meniscus is completed, the droplets of particle suspension are transferred to the substrate. Surface tension force of the printing head surface and the substrate are crucial factors in this step. While the extruded fluid meniscus is in contact with the substrate, the surface tension force of the substrate attracts a fraction of the fluid and picoliter scale droplets are transferred to the substrate after the pinch-off of the droplet. When the printing head surface was hydrophilic (water $\theta_c$ ~ 50°), the fluid wet the head surface and transfer of the droplets did not occur. When a printing head surface was hydrophobic (water $\theta_c$ ~ 109°) and the substrate was hydrophilic (water $\theta_c$ ~ 50°), high surface tension force of the substrate attracted the fluid and most of the fluid overflowed to the substrate and droplets were merged altogether. When both the head surface and the substrate were hydrophobic, surface tension force balance between the substrate and the head was achieved and picoliter scale droplets were transferred from the head to the substrate successfully. Also, when large volume of bulk suspension was loaded to the printing head, gravity-field force overwhelms the surface tension force of the fluid-meniscus and overflow of the fluid to substrate was observed during contact. The relative ratio of the gravity force of a global droplet contained in the printing to the surface tension force of the solvent is

given by: Bond number, $Bo = \frac{\rho g R^2}{\sigma} = \frac{\text{Gravity force}}{\text{Surface tension force}}$ where $\rho$ is the density of the solvent, g is the gravity acceleration, R is the radius of the global droplet, and $\sigma$ is the surface tension force of the solvent. When 10 µl volume of the bulk suspension was used with 200 µm pore size of the head, Bo was calculated to be on the order of $10^{-1}$. In this case, the transferred droplets were merged together to form a single droplet and separation of the individual droplet was not achieved. However, when 0.1 µl volume was used, the corresponding Bo was calculated to be on the order of $10^{-3}$ and each droplet was separated implying that there exists a maximum threshold Bo number for the separation to occur. Generally, the volume of the loaded suspension does not affect the diameter of the transferred droplet on a surface significantly as long as the droplet merge does not occur. The volume of bulk suspension, pore size of the printing head and surface tension energy of the surface are critical parameters for the gravitational force, the surface tension force, and the viscous force to be placed in a right regime to accomplish successful transfer of the droplets. It is observed that the types of solvents, the types of the particles and the volume fraction of the particles affect the diameter of the transferred droplet since those factors determine the viscous and gravitational forces of each droplet. Creating a phase diagram for dimensionless parameters by incorporating various parameters of the suspension to predict the feasibility of the contact printing would be interesting subject of future work. Detailed calculations for this scaling analysis and pressure loss are included in supporting information.

**Rapid Evaporative Self-Assembly of Micro, nanoparticles on a Hydrophobic Surface**

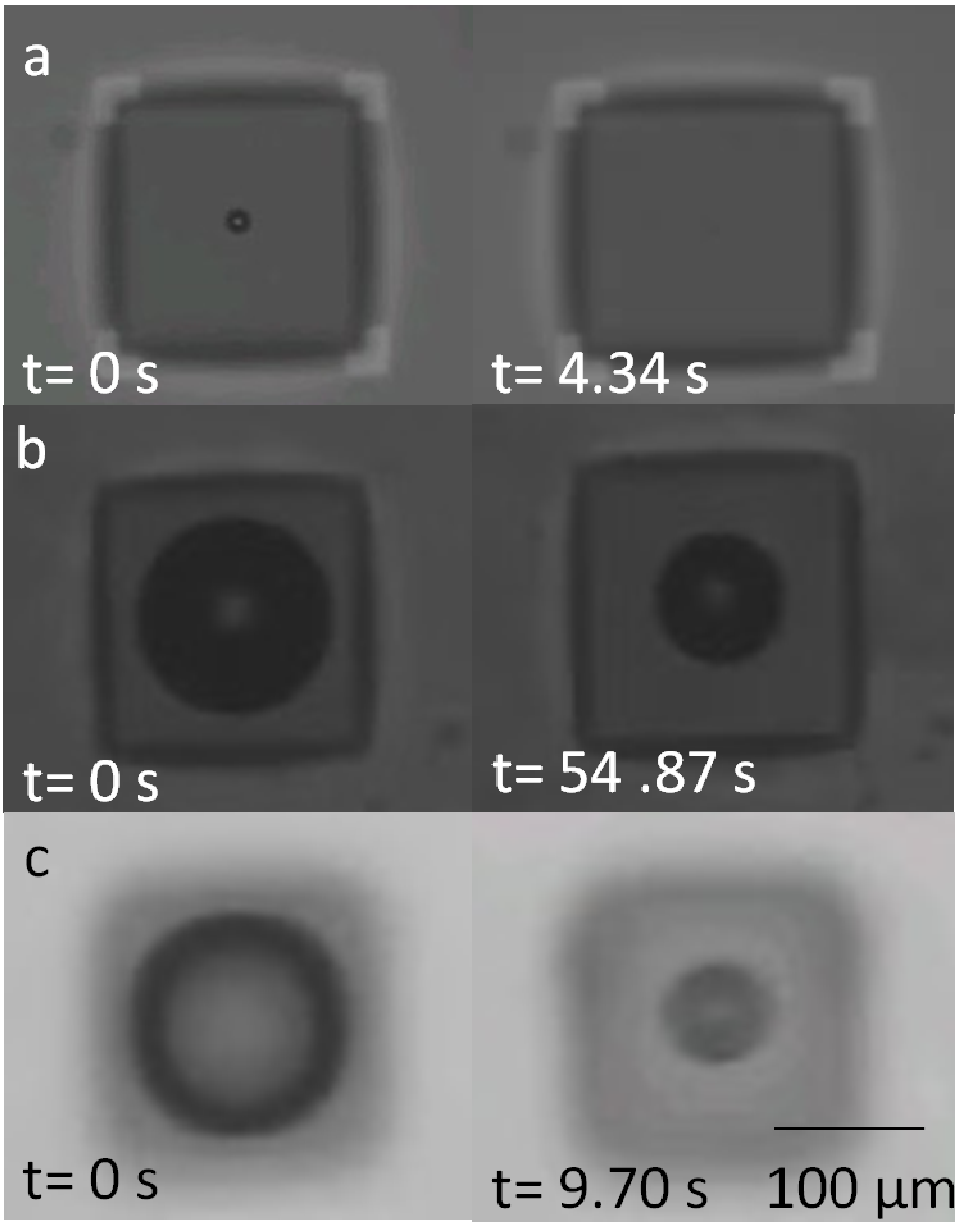


**Figure 2**. Optical snopshots of evaporating droplets after the pinch-off. (left) Right after the pinch-off. (right) After the completion of the evaporation. **a.** Evaporation of 5 $\times 10^{-3}$ wt% gold nanoparticle suspension. A zoomed-in image is found in Figure 4-d(iv). **b.** Evaporation of 1 wt% zinc oxide nanoparticle suspension. **c.** Evaporation of 0.25 wt% zinc oxide nanoparticle suspension.

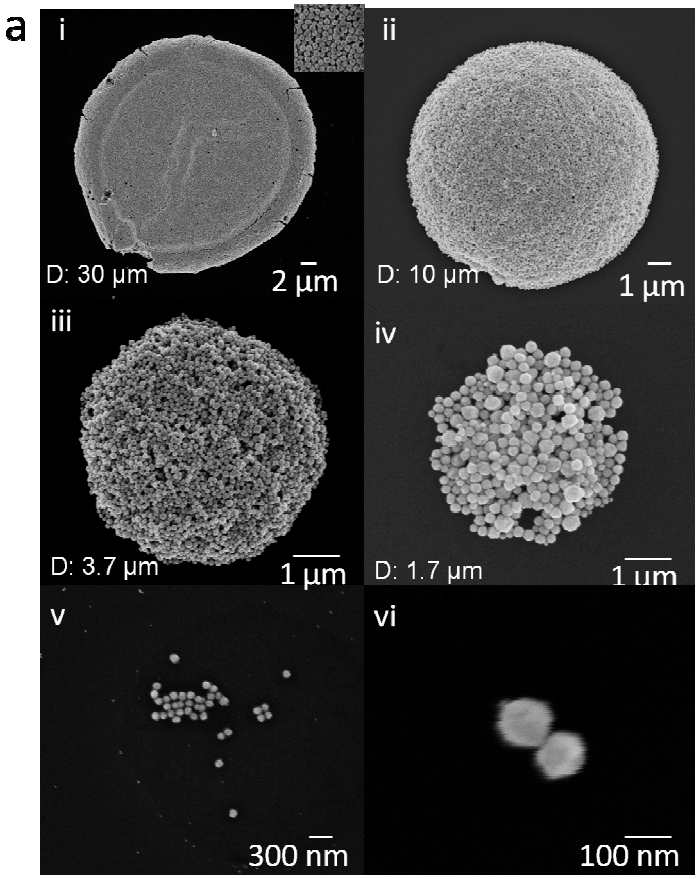
a
i
D: 30 µm
2 µm
ii
D: 10 µm
1 µm
iii
D: 3.7 µm
1 µm
iv
D: 1.7 µm
1 µm
v
300 nm
vi
100 nm

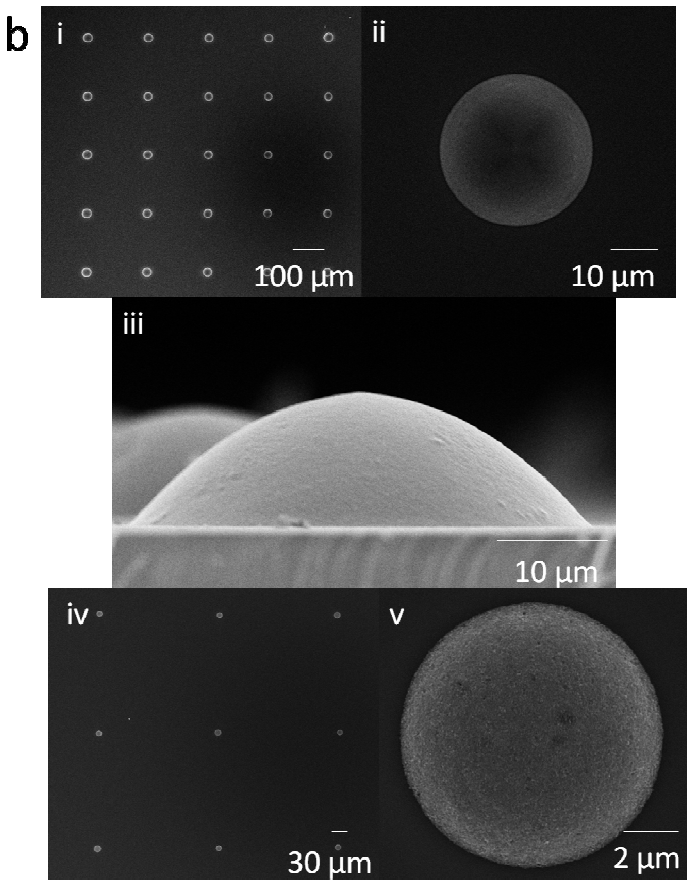
b
i
100 µm
ii
10 µm
iii
10 µm
iv
30 µm
v
2 µm

**Figure 3.** SEM views of nanoparticle clusters. **a.** Gold nanoparticle (diameter ~ 100 nm) clusters printed from 200 μm head pore size. (i) A 30 μm diameter cluster printed from $5 \times 10^{-1}$ wt%. (ii) A 10 μm diameter cluster printed from $5 \times 10^{-2}$ wt%. (iii) A 3.7 μm diameter cluster printed from $5 \times 10^{-3}$ wt%. (iv) A 1.75 μm diameter cluster printed from $5 \times 10^{-4}$ wt%. (v) Dispersed particle clusters printed from $5 \times 10^{-5}$ wt%. (vi) A bi-particle cluster printed from $5 \times 10^{-6}$ wt%. **b.** Zinc oxide nanoparticle (diameter ~ 30 nm) clusters. (i-iii) 30 μm diameter clusters printed from 40 μm head pore size and 40 wt% concentration suspension. (i) High-throughput nanoparticle clusters. (ii) A close view of a single cluster. (iii) A cross sectional view of a single pattern (iv,v) 8 μm diameter clusters printed from 40 μm head pore size and 1 wt%. (iv) High-throughput nanoparticle clusters (v) A close view of a single cluster.

Evaporative self-assembly of micro, nanoparticles on a hydrophobic surface is a key phenomenon in forming 3 D, high-aspect ratio particle clusters. It was previously reported that particles in colloidal suspensions form defect-free, 3 D lattices after evaporation of the drops on hydrophobic surfaces.[17, 21, 23, 30-37] Although some works featured rapid assembly during the formation of the lattices[31, 35, 37], quantitative, systematic studies of the evaporative self-assembly on a hydrophobic surface have not been performed due to lack of experimental platforms to observe evaporation processes. In this work, high optical transparency of a thin membrane of the printing head and low-concentrated suspensions enabled the real-time observation of the convective motion of particles through the optics in the system. Although it is still challenging to identify the exact particle clustering time, the time required for the evaporation of the picoliter-scale droplets, which is very valuable information to examine the kinetics of evaporative self-assembly of the particles, was able to be acquired through this method. Evaporation of picoliter-scale droplets of nanoparticle (100 nm Gold, 30 nm zinc oxide) suspension was monitored by optical microscope in the system. Video clips for pinch-off and evaporation of picoliter-scale droplets of 0.005 wt % Au nanoparticle suspension, 0.25 wt % ZnO nanoparticle suspension, and 1 wt % ZnO nanoparticle suspension are available in Supporting Video 1,2,3, accordingly. Once the picoliter-scale droplet was generated by contacting the printing head with the substrate and following droplet pinch-

off, contact line of the droplet receded very fast and the evaporation of the droplet was completed by forming particle deposits at the center of initial droplet-contact line as shown in Figure 2 a. Generally, from macro to microliter scale of the droplet, either ring deposits are generated at the perimeter of the droplet by coffee-ring effect in case of high fraction suspension[20, 38, 39] or non-uniform deposits are generated inside the perimeter by Marangoni effect[20, 40]. According to the literatures[41-43], there are exceptional cases where a partial fraction of the particles are centered along with coffee ring deposits at certain special conditions, however, complete centering of all particles has not been reported yet. This is attributed to the fact that previous printing technologies were not capable of monitoring both the generation and the evaporation of picoliter-scale droplets of low concentrated-particle suspension simultaneously in-real time. This unique evaporating characteristic is explained by the scaling effect of picoliter scale droplets. Evaporation time of a droplet scales quadratically with length-scale of the droplet. [44, 45] In evaporating, picoliter scale droplets on a hydrophobic surface, the evaporative rate is 100 times faster than microliter scale droplets and the evaporation proceeds by shrinking the contact line at constant contact angle mode[44]. In this mode, the transport of the particles is mainly dominated by the evaporation of the droplet, not the convective transport induced by hydrodynamic effect or thermal gradient of the droplet-Marangoni effect. Along with shrinking perimeter by evaporation, all particles in the droplet are centered. Generally, hydrophillic particles such as gold nanoparticles or silica microparticles, are not attracted to the hydrophobic substrate. Instead, dominant inter-particle forces such as electrostatic forces or van dear waals force cluster the particles during the evaporation of the droplet.[20] If the evaporation time is longer than clustering time, all particles are clustered first and centered after the completion of the evaporation. However, if the particle concentration is extremely low, inter-particle forces decrease and clustering of the particle proceeds slowly. Assuming that the change of low volume (weight) fraction of the particles does not affect the evaporation time of the fluid, there could exist a critical concentration where the deposition of the particles on the substrate is initiated before clustering of the particle is completed. In Figure 3 a, centering of the particles was observed until

particle fraction of $5 \times 10^{-4}$ wt% and dispersed clusters were observed from particle fraction of $5 \times 10^{-5}$ wt%. It implies that the critical concentration for this particular system lies between those two concentrations. However, when hydrophobic particles such as zinc oxide particles were used, the particles are also attracted to the hydrophobic substrate. In this case, the particles are pinned at the contact line when the particle concentration of the droplet reaches to critical concentration.[39] As shown in Figure 2 b-c, when the concentration was very high, up to 40 wt%, the pinning of the particles occurred immediately after the droplet was transferred to the substrate. However, when the concentration was low, down to 1 wt%, the evaporation of the suspension had proceeded first and the pinning of the particle begun when particle concentration inside the droplet reached to the critical concentration required for contact-line pinning. As a result, different concentrations of the particle suspension caused different timing of contact-line pinning. When the contact-line pinning was initiated earlier, the zinc oxide nanoparticle clusters of larger diameters were printed while the clusters of smaller diameters were when the pinning began later as shown in Figure 2 b-c and Figure 3 b. Along with the initial volume fraction of the particles in the original suspension, initial timing for contact line pinning determines the diameter of the zinc oxide nanoparticle clusters. Also the cross-sectional view of the zinc oxide nanoparticle clusters shows that its high-aspect ratio is lower than that of the gold nanoparticle clusters because some fraction of the zinc oxide nanoparticles were deposited downward and overall shape of the structures became widespread while all the gold nanoparticles were centered and formed the high-aspect ratio clusters. The pitch of the clusters was determined by lithographically defined pitch of the pores of the printing head and the size of the clusters was controlled by the volume fraction of the particles in the suspension and solvent drying behavior during the evaporation.

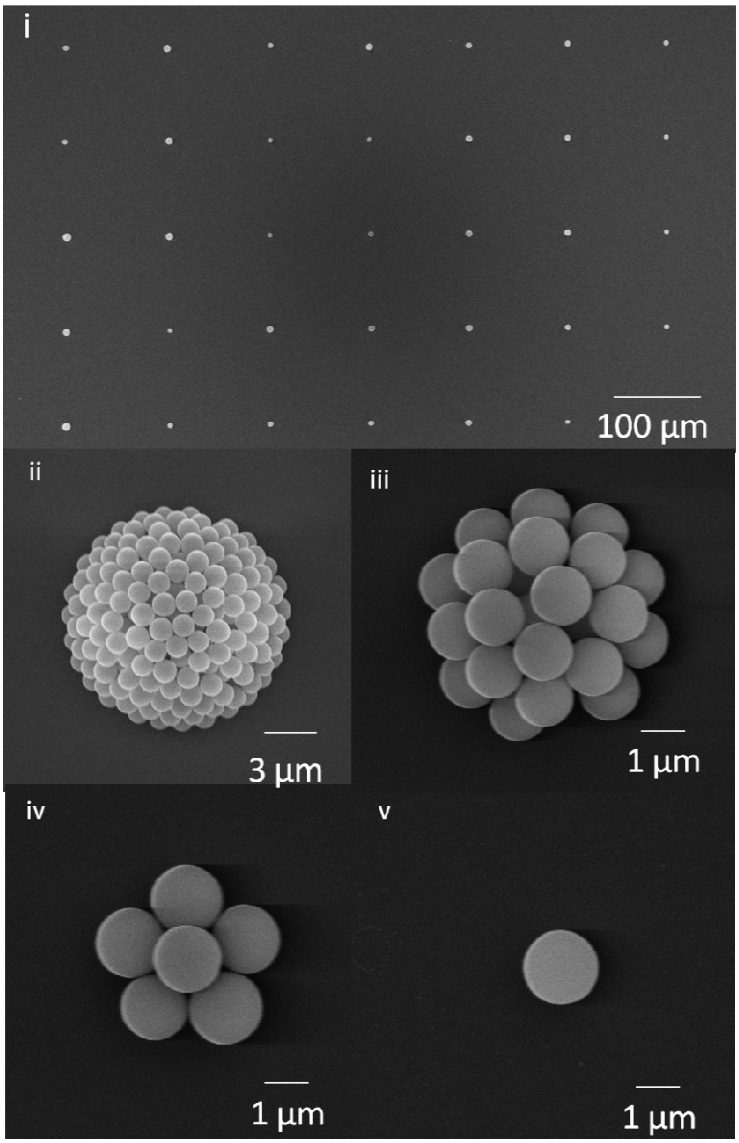
i
100 µm
ii
3 µm
iii
1 µm
iv
1 µm
v
1 µm

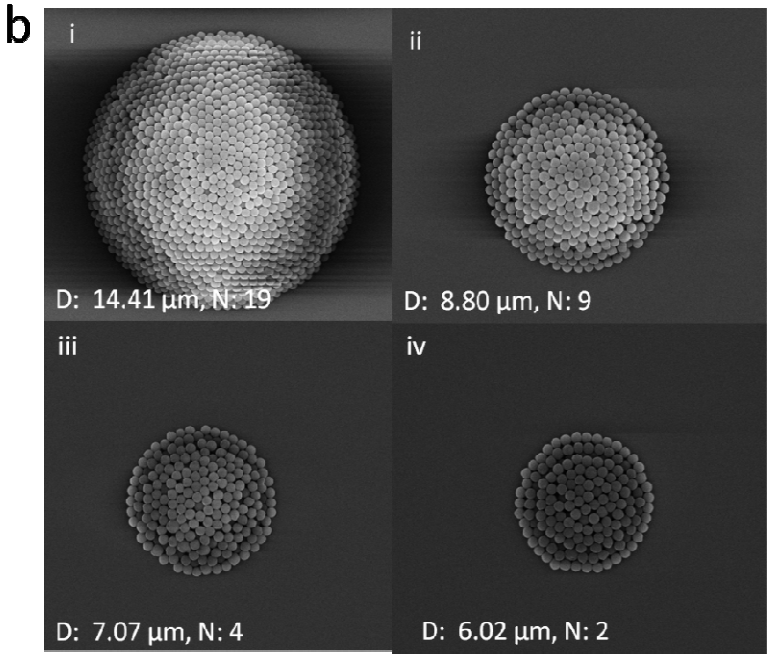
b
i
D: 14.41 µm, N: 19
ii
D: 8.80 µm, N: 9
iii
D: 7.07 µm, N: 4
iv
D: 6.02 µm, N: 2

**Figure 4.** SEM views of microparticle clusters. **a.** silica microsphere (diameter ~ 1 μm) clusters. (i) High-throughput clusters. (ii) A 10 μm diameter-cluster printed from 20 μm head pore size and 5 wt% (particle fraction) concentration. (iii) A 5 μm diameter-cluster printed from 20 μm head pore size and 2 wt% (particle fraction) concentration. (iv-v) Clusters printed from 20 μm head pore size and a wt% (particle fraction) concentration. (iv) A 5-particle cluster. (v) A single particle. Note that the number range of particles are from 1 ~5 for entire area. This variation is caused by inherent statistical distribution of captured particle numbers per each pore. **b.** polystyrene microsphere (diameter ~ 1 μm clusters). Clusters printed from (i) 0.34 wt % (ii) 0.68 wt % (iii) 1.35 wt % (iv) 2.70 wt % concentration. The number of layers, N, is corresponding to the center of the patterns.

Arrays (~ 100 patterns) of microparticle (silica, polystyrene microparticles) clusters were printed on a hydrophobic substrate as demonstrated in Figure 4. Contact-line pinning of the particles did not occur because the hydrophilic particles were not attracted to the substrate. By simply diluting or concentrating the suspension, the size of the cluster was controlled. Contrary to the gold nanoparticle clusters, a critical concentration where clustering of the particles stops was not observed and even a single particle was centered. It is speculated that the lowest particle concentration, 1 wt%, still generates sufficient inter-particle forces to cluster particles within the evaporation time of the droplets. Clustering behavior of various particles in picoliter scale droplets is expected to generate numerous subjects of studies on fundamental colloidal science. Also, with this method, most of micro, nanostructures, or even biological particle clusters such as protein clusters, DNA clusters with any size and spacing will be able to be created on a hydrophobic surface.

## Multiplexed Printing of Micro, nanoparticle Clusters

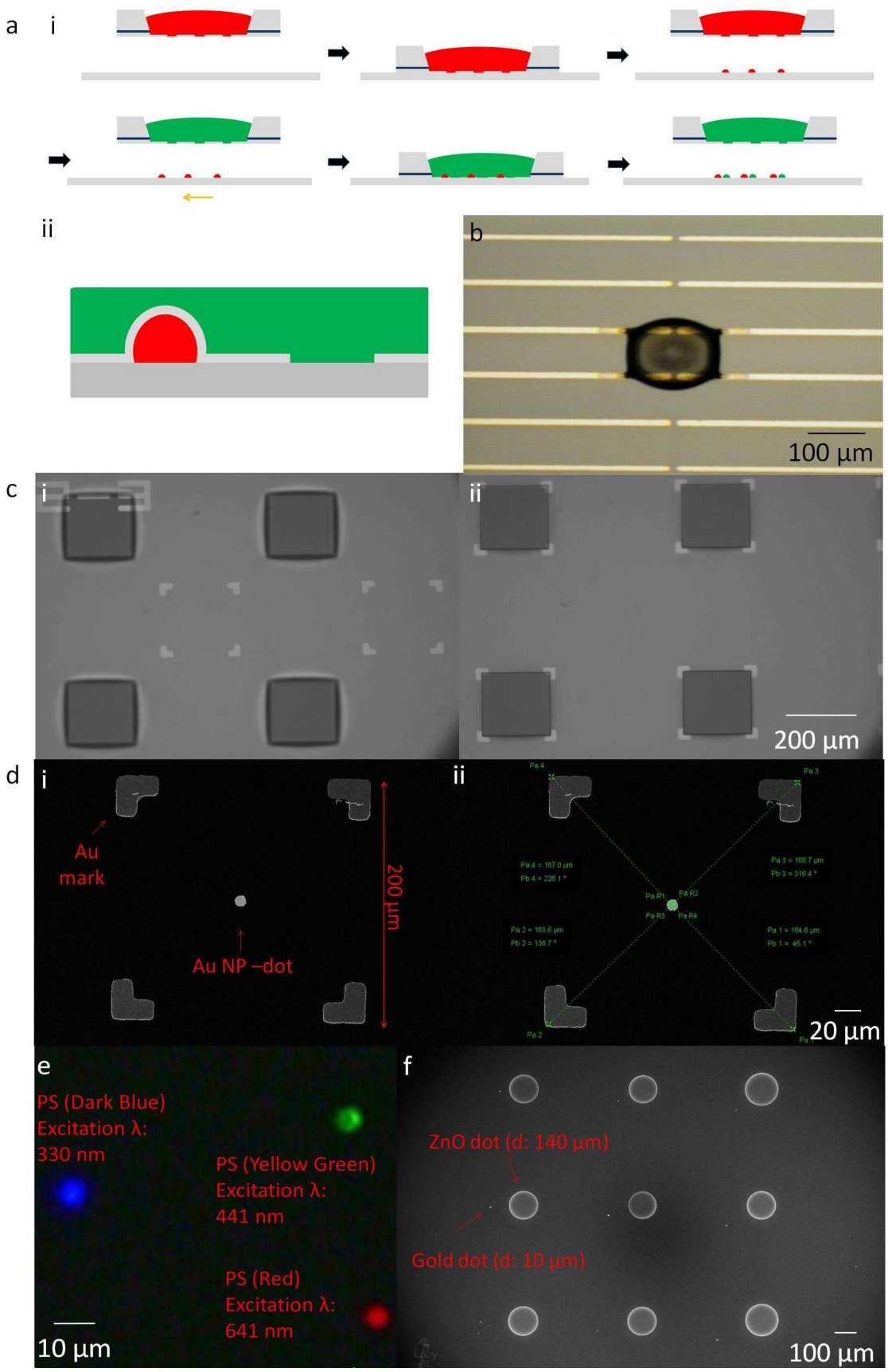


**Figure 5**. Multiplexed printing of micro, nanoparticle clusters. **a.** Schematics of multiplex printing

procedures. (i) A schematic of a series of printing methods. After an initial printing, the next step printing is achieved after the alignment of the head is achieved. (ii) An illustration of a deformed head membrane according to the previously printed clusters. **b.** A zinc oxide nanoparticle cluster (diameter: 40 nm) printed on gold electrodes (thickness: 25 nm) with alignment. The suspension concentration is 40 wt %. **c.** Top views from the printing head side. (i) Before alignment. (ii) After alignment. Alignment is achieved by manipulating a micro-precision stage. **d.** SEM views of gold nanoparticle clusters (diameter: 100 nm) (i) A centered gold nanoparticle cluster with respect to gold alignment marks. (ii) An analyzed image of alignment accuracy. The accuracy is approximately 4 μm. **e.** Layover images of three different fluorescence images. Three different combinations of excitation filter and emission filter were used to acquire four different types of fluorescence light. **f.** Multi-step printing of zinc oxide nanoparticle (diameter: 140 μm) and gold nanoparticle clusters (diameter: 10 μm). Smaller clusters were printed first to prevent breaking the membrane.

A flexible membrane allowed the deformation of the head according to the previous clusters as illustrated in Figure 5 a. At given high aspect ratio, 0.33, a membrane (thickness: silicon: 100 nm, silicon nitride: 100 nm) was able to be conformed to 14 μm-height structure without breaking. Video clips for testing the flexibility of the membrane with ZnO clusters of 60 μm and 13 μm height are available in Supporting Video 4, 5. Multi-layer process capability was demonstrated by printing zinc oxide nanoparticle clusters on gold electrodes. For the droplets of highly concentrated (~ 40 wt%) suspensions, contact line of the droplet was pinned and nanoparticles were continuously deposited on the electrodes-substrate interface as shown in Figure 5 b. A thin, single crystalline porous silicon membrane of the printing head has optical transparency over the visible light spectrum and the location of the printing head was monitored by optical microscope through the membrane. The location of the head was controlled by micron-axis stage of the stage as presented in Figure 5 c-d. The accuracy was realized to the equivalent level of conventional contact photolithography (~ 4 μm). A video clip for serial positioning and printing of gold nanoparticle clusters is available in Supporting Video 6. Also, as

shown in Figure 5 e-f, the alignment of the clusters with respect to previously printed clusters was demonstrated. Multiplex printing of fluoro-microsphere clusters with different excitation/emission wavelengths were performed and visualized by fluorescence microscopy. Also, gold and zinc oxide nanoparticle clusters were printed on a target spot and the clusters were accurately positioned. Smaller patterns were created first to prevent the breaking of the membrane.

**Study on Size-uniformity of Particle Cluster Arrays by SERS Measurement**

Size-uniformity of large arrays of gold nanoparticle clusters was thoroughly analyzed by Surface Enhanced Raman Spectroscopy (SERS) measurement. Usually, commercially available metallic nanoparticle suspension contains very low fractions of nanoparticles due to the presence of strong attractive inter-particle forces and high material costs. Typically, SERS measurement is performed on naturally evaporated deposits of metallic nanoparticles. Thickness variation of the deposits is randomly fluctuating because natural evaporation of a suspension droplet does not provide any means to control geometry of the deposits. Also, a large volume of suspension is required to generate thicker deposits for stronger signal intensity. With the presented method, high-aspect ratio, gold nanoparticle (diameter: 100 nm) clusters of various sizes (diameter~ 30 µm, 10 µm, 3.7 µm, 1.75 µm) were printed from low volume suspension (0.5 ~ 1.0 µL) of low particle fraction ($5\times10^{-4}$ wt % ~ $5\times10^{-2}$ wt %). The printed clusters were immersed in trans-1,2-bis(4-pyridyl)-ethylene (BPE) solution for 2 hours prior to the measurement.

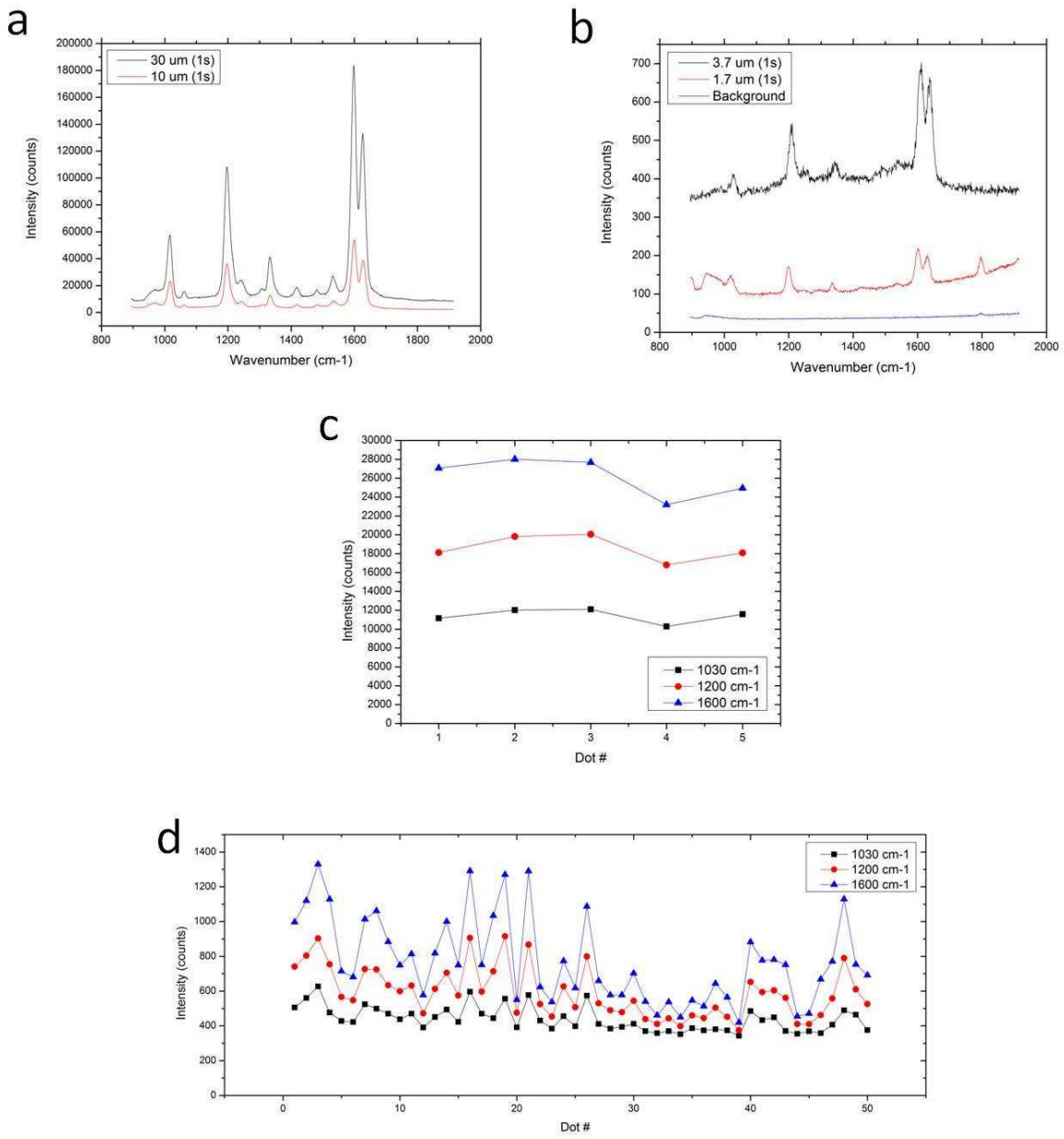


**Figure 6. a-b**. Surface Enhanced Raman Spectroscopy (SERS)-spectrum of trans-1,2-bis(4-pyridyl)-ethylene (BPE) molecules-absorbed on gold nanoparticle clusters. **a.** Spectrum from 30 µm and 10 µm diameter gold nanoparticle clusters. **b.** Spectrum from 3.7 µm and 1.75 µm diameter gold nanoparticle clusters and background substrate. The signal intensity drastically increases as the diameter increases. **c-d**. SERS signal intensity variation of the high-throughput gold nanoparticle clusters for size-uniformity characterization. **c.** 5 gold nanoparticle clusters (average diameter: 10 µm). **d.** 50 gold dots

(average diameter: 3.7 μm).

As shown in Figure 6, strong, uniform SERS signal was obtained from gold nanoparticle clusters. In Figure 6 a-b, the intensity of SERS signal from the cluster was significantly modulated by the small change of cluster size. The magnitude of the order of the signal intensity changed $10^6$ times as the diameter scaled up 10 times. The result implies that the intensity of SERS signal from the cluster is a good measure to identify size-uniformity of the cluster arrays. The size-uniformity of the clusters was analyzed by measuring SERS signal of the clusters as presented in Figure 6 c-d, The clusters of two different sizes (Diameter: 10 μm, 3.7 μm) were used for the measurement. The deviation of the signal is less than ±10% from the measurement on 5 clusters of 10 μm diameter. Also, the measurement on 50 clusters of 3.7 μm diameter shows the deviation was around ±10 ~ 50 %. The intensity of SERS signal is roughly proportional to the number of molecules attached to the particle surfaces and the signal is also proportional to the volume of the patterns, which means the signal scales cubically with length of the cluster. This argument leads to the estimates that variation of the cluster diameter is within 20 % in the array. We anticipate that this uniformity will be greatly improved if an additional pressure source is implemented to the printing head for flattening inherent meniscus effect of the suspension. These preliminary measurement results show good potential to apply this method to manufacture micro-scale devices in material science with low material consumption.

## CONCLUSION

A fast method to create high-throughput, size-tunable micro, nanoparticle clusters is developed by applying evaporative-self assembly to picoliter scale droplets of particle suspension. Formation of the droplets from a nano-fabricated printing head is driven by gravity force and surface tension force of a

contacting surface. Fast evaporation of the droplets on a hydrophobic surface drives the fast, complete clustering of the particles when the particle clustering time is shorter than the evaporation time of the droplet. Based on this method, multiplex printing of various particle clusters is demonstrated with accurate positioning and alignment capability. Size-uniformity of the large cluster arrays is examined by SERS measurement and demonstrated to be fine. The presented method provides new revenues to study fundamental colloidal science in a more controllable way and also show potential to manufacture micro, nanoparticle devices in material science with low material processing cost.

## METHODS

**Materials.** A liquid suspension of silica microspheres (Silicon dioxide-based micro particles; diameter, 1, 3, and 5 μm; water, 95 wt %; silica: 5 wt %, Sigma-Aldrich) and a liquid suspension of fluorescent microspheres (Fluoresbrite Carboxylate$^{R}$; diameter, 0.5 μm; excitation wavelength maxima: 360 nm, 441 nm, 529 nm, 641nm; water, 97.5 wt %; polystyrene microspheres: 2.5 wt %, Polysciences, Inc.) was diluted into various concentrations of suspension (1.25, 0.625, and 0.3125 wt % solutes). Zinc oxide nanoparticles (diameter, 30 nm; water, 60 wt %; ZnO, 40 wt %; MK nano) were diluted into various concentrations of suspension (2.5, 1.25, 0.625, and 0.3125 wt % solutes) by adding a controlled volume of deionized water. A liquid suspension of gold nanoparticles (diameter, 100 nm; water, 99.995 wt %, Au, $5 \times 10^{-3}$ wt %; Nanopartz) was diluted into various concentrations of suspension ($5 \times 10^{-4}$ wt %, $5 \times 10^{-5}$ wt%, Au nanoparticles) and also was concentrated by 10 times ($5 \times 10^{-2}$ wt %, Au nanoparticles).

**Fabrication of the printing heads.** A 6 inches-Silicon-on-Insulator (SOI) wafer (Top device layer: silicon 100 nm, Buried oxide layer: silicon dioxide 400 nm, Base: silicon 650 μm, *SOITEC*, France) was used for the fabrication of the printing head. The backside of the SOI wafer was grinded by 400 μm to reach the final thickness of 250 μm and polished. Low-stress silicon nitride film of 35 nm was deposited on both sides of the wafer by Low-Pressure Chemical Vapor Deposition (LPCVD) for

generating masking materials of wet-etching process. Then, back-side of the wafer was spin-coated with photoresist and baked at 120 C for 5 min and placed in Buffered-Oxide-Etcher (BOE, BHF: DI water = 10:1) for 10 hours to etch the silicon nitride layer of top-side of the wafer. After complete etching of the silicon nitride layer on the top-side, the photoresist was removed by photoresist removal (PRS-3000, *J.T. Baker*, USA) overnight. The wafer was diced into 1 cm ×1 cm dies and both top and back sides of each die were coated with photoresist. Photolithography was performed on top-side to define holes for a porous membrane of the printing head and Reactive-Ion Etching to etch top side silicon through the defined photo-patterns was followed by taking advantage of buried oxide as an etch-stop layer. After the removal of the photoresist, the top and backsides of the chip were coated with photoresist and reservoir area of the bulk suspension was defined by photolithography followed by RIE etching to open area for silicon wet-etching. Before wet-etching of bulk silicon layer, top-layer was coated with 10 µm-thickness protective polymer (ProTEK B3, *Brewer science*, USA) to protect porous membrane structures on top-side from being etched by wet-etchant. The prepared chips are wet-etched for 4 hours in the bath where 15 Liter of 5 % Tetramethylammonium hydroxide (TMAH) solution was prepared at 90 C°. After wet etching is completed, the protective polymer was removed by PRS-3000 / IPA / water rinse and BOE etching (5:1 BHF, 5 minute at room temperature) was followed to etch a buried oxide layer completely. By design, thin, microporous membrane is released where the area of the membrane is 2 mm × 2 mm. The membrane side of the fabricated devices was treated by oxygen plasma (300 Watt, 250 mTorr, 1 minute) to eliminate possible residue of protective polymer and the devices were placed on hot plate at 120 C° overnight to neutralize charge state of the membrane surface from hydrophilic state. Finally, the fabricated printing heads were coated with Fluoroctatrichlorosilane (FOTS) monolayer by Metal-Organic Chemical Vapour Deposition (MOCVD) to maintain the top side of membrane hydrophobic.

**Fabrication of the handling wafer.** A 4 inch-silicon wafer (Lightly p-type doped, Thickness: silicon 500 µm) was used for the fabrication of the handling wafer. Low-stress silicon nitride film of 35 nm was

deposited on both sides of the wafer by Low-Pressure Chemical Vapor Deposition (LPCVD) for generating masking materials of wet-etching process. Top side of the wafer was coated with photoresist. Photolithography was performed on top-side to define a wafer-through hole (6 mm × 6 mm square) and Reactive-Ion Etching of silicon nitride layer through the defined photo-patterns was followed to define etching area. The wafer is wet-etched for 16 hours in the bath where 15 Liter of 5 % Tetramethylammonium hydroxide (TMAH) solution was prepared at 90 C°. After wet etching is completed, the protective polymer was removed by PRS-3000 / IPA / water rinse and the surface of the wafer was cleaned by oxygen plasma (300 Watt, 250 mTorr, 1 minute) to eliminate the residue of the protective polymer.

**Fabrication of the printing head- handling wafer complex.** At first, a fabricated handling wafer was spincoated with photoresist. The printing head is placed on the center of handling wafer in a way that the membrane of the printing head is exposed to air without any blocking. Then, the printing head - the handling wafer with photoresist complex are baked together at 120 C° for 1 minute on hot plate with heavy load press to promote the adhesion between the printing head and the handling wafer.

**Micro, nanoparticle printing.** A printing head – handling wafer complex was attached to a mask holder of uv-exposure system for contact- photolithography (MA/BA6, Suss MicroTec, Germany) via vacuum. The mask holder was inserted to the system and a substrate for printing was loaded to the stage. After loading the substrate, the alignment of the printing head to the patterns on the substrate wafer was performed and the spacing gap between the printing head and the substrate was controlled and placed by taking advantage of the embedded electronics of the system. The minimum threshold gap was a half of the width of pore size of the membrane. The micro, nanoparticle suspension was loaded to the reservoir of the printing head. Initially, 10 µl volume of the suspension was loaded by micro-pipette to the reservoir forming a circular contact line of an overflowed droplet on top of the fluid-cell as shown

in Figure S1. Then, the meniscus of the suspension was flattened by drawing excessive volume of the suspension to ensure two-dimensional symmetry of the meniscus surface is not perturbed. A thin, glass cover-slide was capped on the mask holder to prevent the evaporation of the suspension during printing. The contact of the extruded membrane of the printing head was performed by driving the mask holder to the substrate. After 1 second of the contact, the printing head was driven back to the original position and the evaporation of the printed droplets were observed in-real time by optical microscope embedded in the printing system in case the concentration of the suspension was sufficiently low to be transparent. After the evaporation of the droplets was completed, the substrate with printed patterns was unloaded.

**Fluorescence imaging set-up and image analysis.** Fluorescence imaging was performed using a Nikon TE 2000 inverted fluorescence microscope. A different filter cube is used for each microparticle to match the emission and excitation wavelengths. The acquired images were overlaid to obtain the final image. Obtained fluorescence images are analyzed by free software, Pixel View (Global Systems Science, Regents of the University of California). Each pixel of the image is dissected into Red, Green, Blue component color intensity (%) by this software. Blue color intensity of the inner-most pixel of the images from polystyrene beads with dark blue fluorescence tags was analyzed to perform calibration the number of polystyrene beads versus blue color intensity.

**Surface Enhanced Raman Spectroscopy (SERS) measurement set-up.** The SERS measurements were performed with a Raman setup built around an inverted microscope (Nikon TE2000). A 10x objective lens was used to focus the laser (785 nm, 30 mW) onto the sample and collect the SERS signal. The collected signal is passed onto a spectrometer (Princeton Instruments, SP2300) for detection.

**Table 1.** Summary of data shown in Figure 6 c-d.

| Wave number (cm -1) | 3.7 μm diameter patterns (50 dots) | | |
|---|---|---|---|
| | Average Intensity (count) | Standard deviation | Uniformity (%) |
| 1030 | 439 | 70.9 | 16.2 |
| 1200 | 591 | 145 | 24.6 |
| 1600 | 776 | 249 | 32.0 |
| **Wave number (cm -1)** | **10 μm diameter patterns (5 dots)** | | |
| | Average Intensity (count) | Standard deviation | Uniformity (%) |
| 1030 | 11428 | 744 | 6.51 |
| 1200 | 18577 | 1350 | 7.29 |
| 1600 | 26180 | 2050 | 7.84 |

For full guidelines, please see the Guide, Notes, Notice, or Instructions for Authors that appear in each publication's first issue of the year and on the World Wide Web at http://pubs.acs.org. This may include an introduction, experimental details (sections titled Experimental Methods, Experimental Section, or Materials and Methods), theoretical basis (sections titled Theoretical Basis or Theoretical Calculations), results, discussion, and conclusions.

ACKNOWLEDGMENT

This work was supported by a grant (2009K000069) from Center for Nanoscale Mechatronics & Manufacturing (CNMM), one of the 21st Century Frontier Research Programs, which are supported by Ministry of Education, Science and Technology, Korea. S. Choi also gives thanks for his graduate fellowship from Samsung Scholarship Foundation.

**Supporting Information Available:** Detailed calculations for scaling analysis and pressure loss calculation based on fluid mechanics, and estimating the number of the nanoparticle clusters, n, in 30

μm diameter clusters are available in supporting information.

REFERENCES

1. Joannopoulos, J. D.; Villeneuve, P. R.; Fan, S., Photonic crystals: putting a new twist on light. *Nature* **1997,** 386, (6621), 143-149.

2. Norris, D. J., Photonic Crystals: A view of the future. *Nat Mater* **2007,** 6, (3), 177-178.

3. Hynninen, A.-P.; Thijssen, J. H. J.; Vermolen, E. C. M.; Dijkstra, M.; van Blaaderen, A., Self-assembly route for photonic crystals with a bandgap in the visible region. *Nat Mater* **2007,** 6, (3), 202-205.

4. Ahn, B. Y.; Duoss, E. B.; Motala, M. J.; Guo, X.; Park, S.-I.; Xiong, Y.; Yoon, J.; Nuzzo, R. G.; Rogers, J. A.; Lewis, J. A., Omnidirectional Printing of Flexible, Stretchable, and Spanning Silver Microelectrodes. *Science* **2009,** 323, (5921), 1590-1593.

5. Briseno, A. L.; Mannsfeld, S. C. B.; Ling, M. M.; Liu, S.; Tseng, R. J.; Reese, C.; Roberts, M. E.; Yang, Y.; Wudl, F.; Bao, Z., Patterning organic single-crystal transistor arrays. *Nature* **2006,** 444, (7121), 913-917.

6. Aoki, K.; Guimard, D.; Nishioka, M.; Nomura, M.; Iwamoto, S.; Arakawa, Y., Coupling of quantum-dot light emission with a three-dimensional photonic-crystal nanocavity. *Nat Photon* **2008,** 2, (11), 688-692.

7. Noda, S.; Fujita, M., Light-emitting diodes: Photonic crystal efficiency boost. *Nat Photon* **2009,** 3, (3), 129-130.

8. Graham-Rowe, D., From dots to devices. *Nat Photon* **2009,** 3, (6), 307-309.

9. Barnes, W. L.; Dereux, A.; Ebbesen, T. W., Surface plasmon subwavelength optics. *Nature* **2003,** 424, (6950), 824-830.

10. Lal, S.; Link, S.; Halas, N. J., Nano-optics from sensing to waveguiding. *Nat Photon* **2007,** 1, (11), 641-648.

11. Kamyshny, A.; Ben-Moshe, M.; Aviezer, S.; Magdassi, S., Ink-Jet Printing of Metallic Nanoparticles and Microemulsions. *Macromolecular Rapid Communications* **2005,** 26, (4), 281-288.

12. Ko, H.-Y.; Park, J.; Shin, H.; Moon, J., Rapid Self-Assembly of Monodisperse Colloidal Spheres in an Ink-Jet Printed Droplet. *Chemistry of Materials* **2004,** 16, (22), 4212-4215.

13. Park, J.; Moon, J.; Shin, H.; Wang, D.; Park, M., Direct-write fabrication of colloidal photonic crystal microarrays by ink-jet printing. *Journal of Colloid and Interface Science* **2006,** 298, (2), 713-719.

14. Park, J.-U.; Hardy, M.; Kang, S. J.; Barton, K.; Adair, K.; Mukhopadhyay, D. k.; Lee, C. Y.; Strano, M. S.; Alleyne, A. G.; Georgiadis, J. G.; Ferreira, P. M.; Rogers, J. A., High-resolution electrohydrodynamic jet printing. *Nat Mater* **2007,** 6, (10), 782-789.

15. Piner, R. D.; Zhu, J.; Xu, F.; Hong, S.; Mirkin, C. A., "Dip-Pen" Nanolithography. *Science* **1999,** 283, (5402), 661-663.

16. Jamshidi, A.; Neale, S. L.; Yu, K.; Pauzauskie, P. J.; Schuck, P. J.; Valley, J. K.; Hsu, H.-Y.; Ohta, A. T.; Wu, M. C., NanoPen: Dynamic, Low-Power, and Light-Actuated Patterning of Nanoparticles. *Nano Letters* **2009,** 9, (8), 2921-2925.

17. Kraus, T.; Malaquin, L.; Schmid, H.; Riess, W.; Spencer, N. D.; Wolf, H., Nanoparticle printing with single-particle resolution. *Nat Nano* **2007,** 2, (9), 570-576.

18. Yin, Y.; Lu, Y.; Gates, B.; Xia, Y., Template-Assisted Self-Assembly:??A Practical Route to Complex Aggregates of Monodispersed Colloids with Well-Defined Sizes, Shapes, and Structures. *Journal of the American Chemical Society* **2001,** 123, (36), 8718-8729.

19. Choi, S.; Park, I.; Hao, Z.; Holman, H.-y. N.; Pisano, A. P.; Zohdi, T. I., Ultrafast Self-Assembly of Microscale Particles by Open-Channel Flow. *Langmuir* **2010,** 26, (7), 4661-4667.

20. Choi, S.; Stassi, S.; Pisano, A. P.; Zohdi, T. I., Coffee-Ring Effect-Based Three Dimensional Patterning of Micro/Nanoparticle Assembly with a Single Droplet. *Langmuir* **2010,** 26, (14), 11690-11698.

21. Masuda, Y.; Itoh, T.; Koumoto, K., Self-Assembly and Micropatterning of Spherical-Particle Assemblies. *Advanced Materials* **2005,** 17, (7), 841-845.

22. Leichle, T.; Lishchynska, M.; Mathieu, F.; Pourciel, J. B.; Saya, D.; Nicu, L., A Microcantilever-Based Picoliter Droplet Dispenser With Integrated Force Sensors and Electroassisted Deposition Means. *Microelectromechanical Systems, Journal of* **2008,** 17, (5), 1239-1253.

23. Valsesia, A.; Leïchlé, T.; Lacroix, L.-M.; Nicu, L.; Bretagnol, F.; Colpo, P.; Rossi, F.; Bergaud, C., Deposition of Nanobead Hexagonal Crystals Using Silicon Microcantilevers. *Small* **2006,** 2, (12), 1444-1447.

24. Sirringhaus, H.; Kawase, T.; Friend, R. H.; Shimoda, T.; Inbasekaran, M.; Wu, W.; Woo, E. P., High-Resolution Inkjet Printing of All-Polymer Transistor Circuits. *Science* **2000,** 290, (5499), 2123-2126.

25. Park, I.; Ko, S. H.; Pan, H.; Grigoropoulos, C. P.; Pisano, A. P.; Fréchet, J. M. J.; Lee, E. S.; Jeong, J. H., Nanoscale Patterning and Electronics on Flexible Substrate by Direct Nanoimprinting of Metallic Nanoparticles. *Advanced Materials* **2008,** 20, (3), 489-496.

26. Qin, D.; Xia, Y.; Xu, B.; Yang, H.; Zhu, C.; Whitesides, G. M., Fabrication of Ordered Two-Dimensional Arrays of Micro- and Nanoparticles Using Patterned Self-Assembled Monolayers as Templates. *Advanced Materials* **1999,** 11, (17), 1433-1437.

27. Derby, B., Inkjet Printing of Functional and Structural Materials: Fluid Property Requirements, Feature Stability, and Resolution. *Annual Review of Materials Research* **2010,** 40, (1), 395-414.

28. Xiong, X.; Makaram, P.; Busnaina, A.; Bakhtari, K.; Somu, S.; McGruer, N.; Park, J., Large scale directed assembly of nanoparticles using nanotrench templates. *Applied Physics Letters* **2006,** 89, (19), 193108-3.

29. Stringer, J.; Derby, B., Limits to feature size and resolution in ink jet printing. *Journal of the European Ceramic Society* **2009,** 29, (5), 913-918.

30. Mukhopadhyay, R.; Al-Hanbali, O.; Pillai, S.; Hemmersam, A. G.; Meyer, R. L.; Hunter, A. C.;

Rutt, K. J.; Besenbacher, F.; Moghimi, S. M.; Kingshott, P., Ordering of Binary Polymeric Nanoparticles on Hydrophobic Surfaces Assembled from Low Volume Fraction Dispersions. *Journal of the American Chemical Society* **2007,** 129, (44), 13390-13391.

31. Kitaev, V.; Ozin, G. A., Self-Assembled Surface Patterns of Binary Colloidal Crystals. *Advanced Materials* **2003,** 15, (1), 75-78.

32. Bodiguel, H.; Doumenc, F. d. r.; Guerrier, B. a., Stick-Slip Patterning at Low Capillary Numbers for an Evaporating Colloidal Suspension. *Langmuir* **2010,** 26, (13), 10758-10763.

33. Uno, K.; Hayashi, K.; Hayashi, T.; Ito, K.; Kitano, H., Particle adsorption in evaporating droplets of polymer latex dispersions on hydrophilic and hydrophobic surfaces. *Colloid & Polymer Science* **1998,** 276, (9), 810-815.

34. Soboleva, O. A.; Summ, B. D., The Kinetics of Dewetting of Hydrophobic Surfaces during the Evaporation of Surfactant Solution Drops. *Colloid Journal* **2003,** 65, (1), 89-93.

35. Cha, N.-G.; Echegoyen, Y.; Kim, T.-H.; Park, J.-G.; Busnaina, A. A., Convective Assembly and Dry Transfer of Nanoparticles Using Hydrophobic/Hydrophilic Monolayer Templates. *Langmuir* **2009,** 25, (19), 11375-11382.

36. Xu, J.; Xia, J.; Lin, Z., Evaporation-Induced Self-Assembly of Nanoparticles from a Sphere-on-Flat Geometry. *Angewandte Chemie International Edition* **2007,** 46, (11), 1860-1863.

37. Han, W.; Byun, M.; Lin, Z., Assembling and positioning latex nanoparticles via controlled evaporative self-assembly. *Journal of Materials Chemistry* **2011,** 21, (42), 16968-16972.

38. Deegan, R. D.; Bakajin, O.; Dupont, T. F.; Huber, G.; Nagel, S. R.; Witten, T. A., Capillary flow as the cause of ring stains from dried liquid drops. *Nature* **1997,** 389, (6653), 827-829.

39. Deegan, R. D., Pattern formation in drying drops. *Physical Review E* **2000,** 61, (1), 475.

40. Hu, H.; Larson, R. G., Marangoni Effect Reverses Coffee-Ring Depositions. *The Journal of Physical Chemistry B* **2006,** 110, (14), 7090-7094.

41. Suematsu, N. J.; Ogawa, Y.; Yamamoto, Y.; Yamaguchi, T., Dewetting self-assembly of

nanoparticles into hexagonal array of nanorings. *Journal of Colloid and Interface Science* **2007,** 310, (2), 648-652.

42. Andrew, S., Dewetting-mediated pattern formation in nanoparticle assemblies. *Journal of Physics: Condensed Matter* **2011,** 23, (8), 083001.

43. Martin, C. P.; Blunt, M. O.; Pauliac-Vaujour, E.; Stannard, A.; Moriarty, P.; Vancea, I.; Thiele, U., Controlling Pattern Formation in Nanoparticle Assemblies via Directed Solvent Dewetting. *Physical Review Letters* **2007,** 99, (11), 116103.

44. McHale, G.; Aqil, S.; Shirtcliffe, N. J.; Newton, M. I.; Erbil, H. Y., Analysis of Droplet Evaporation on a Superhydrophobic Surface. *Langmuir* **2005,** 21, (24), 11053-11060.

45. Arcamone, J.; Dujardin, E.; Rius, G.; Perez-Murano, F.; Ondarcuhu, T., Evaporation of Femtoliter Sessile Droplets Monitored with Nanomechanical Mass Sensors. *The Journal of Physical Chemistry B* **2007,** 111, (45), 13020-13027.

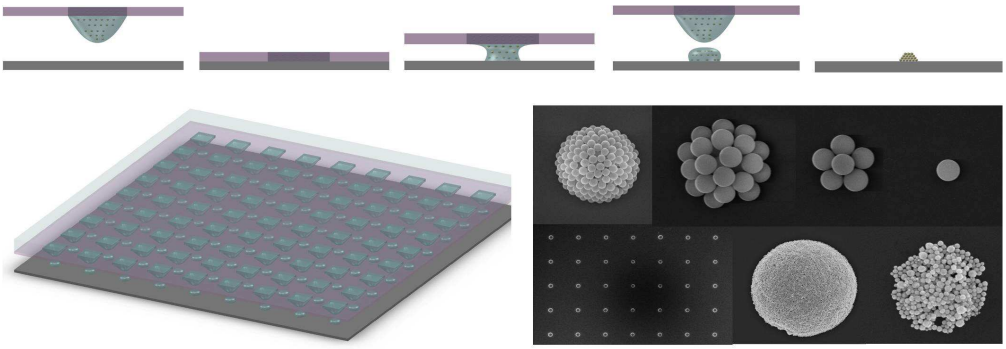

358x123mm (150 x 150 DPI)